

ONE-STEP FACE RESTORATION VIA SHORTCUT-ENHANCED COUPLING FLOW

Xiaohui Sun, Hanlin Wu

School of Information Science and Technology, Beijing Foreign Studies University

ABSTRACT

Face restoration has advanced significantly with generative models like diffusion models and flow matching (FM), which learn continuous-time mappings between distributions. However, existing FM-based approaches often start from Gaussian noise, ignoring the inherent dependency between low-quality (LQ) and high-quality (HQ) data, resulting in path crossovers, curved trajectories, and multi-step sampling requirements. To address these issues, we propose **Shortcut-enhanced Coupling Flow for Face Restoration (SCFlowFR)**. First, it establishes a *data-dependent coupling* that explicitly models the LQ–HQ dependency, minimizing path crossovers and promoting near-linear transport. Second, we employ *conditional mean estimation* to obtain a coarse prediction that refines the source anchor to tighten coupling and conditions the velocity field to stabilize large-step updates. Third, a *shortcut constraint* supervises average velocities over arbitrary time intervals, enabling accurate one-step inference. Experiments demonstrate that SCFlowFR achieves state-of-the-art one-step face restoration quality with inference speed comparable to traditional non-diffusion methods.

Index Terms— Face Restoration, Flow Matching, Data-Dependent Coupling, Shortcut

1. INTRODUCTION

Face restoration aims to recover high-quality (HQ) facial images from degraded inputs and is crucial for photography enhancement, video communication, and biometrics. Recent advances in generative modeling have significantly improved restoration quality, yet a key trade-off between fidelity and efficiency remains.

Diffusion models (DMs) formulate image restoration as a gradual denoising [1, 2]. Methods like DiffBIR [3] and StableSR [4] leverage powerful pretrained diffusion priors to produce highly realistic results. However, they require dozens to hundreds of sampling steps, leading to high latency that hinders real-time deployment [5, 6].

Recently, Flow Matching (FM) [7, 8] has emerged as an efficient alternative that learns deterministic ODE-based transport from a source distribution to a target distribution. FM-based restoration methods [9, 10] typically employ an *independent coupling*, where the source (Gaussian noise) and

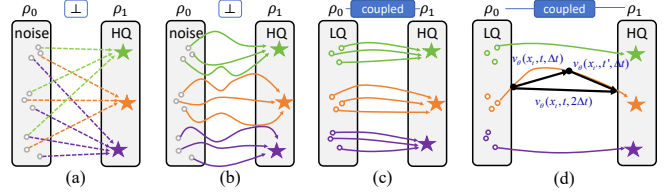


Fig. 1. (a) Linear interpolation under independent marginal assumptions yields intersecting paths. (b) Vanilla FM learns a highly curved velocity field due to lack of source–target dependency modeling. (c) Coupling FM explicitly models dependencies between source and target, producing straighter trajectories. (d) Our SCFlowFR leverages shortcut constraints to learn the averaged velocity between arbitrary time steps, enabling one-step sampling.

the target HQ image are paired without regard to the observed LQ input. This breaks the conditional nature of face restoration tasks, and fails to model the intrinsic dependency between the given LQ image and its corresponding HQ counterpart. As shown in Fig. 1 (a), independently pairing noise and HQ samples can lead to intersecting linear interpolations, producing ambiguous velocity supervision and deviating the learned dynamics from straight transport paths (Fig. 1 (b)). Such misalignment makes single-step inference highly sensitive to discretization errors.

To address the misalignment caused by independent noise–HQ pairing, we propose SCFlowFR, a novel FM framework that explicitly respects the conditional nature of face restoration by establishing a *data-dependent coupling* between source and target. Rather than sampling from an unconditional Gaussian, we construct the source distribution based on the observed LQ image. This coupling significantly reduces path crossovers and promotes near-linear transport dynamics, as illustrated in Fig. 1 (c).

Nevertheless, under realistic degradations such as severe blur or noise, the direct encoding of the LQ input may deviate significantly from the true HQ manifold. Anchoring the source to this unreliable representation reintroduces trajectory curvature. To address this, we employ *conditional mean estimation* using a lightweight predictor trained via least-squares regression to produce a coarse reconstruction from the LQ input. This coarse prediction serves as a refined center for the source distribution, tightening the coupling, and also as

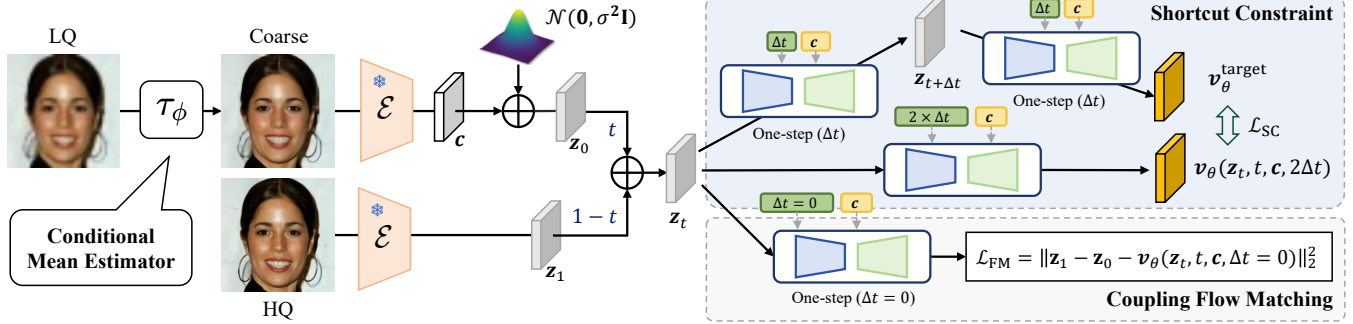


Fig. 2. Overview of the SCFlowFR. We first construct a coupled transport path between the LQ and HQ image distributions (left), and leverage the preliminarily restored image from τ_ϕ as conditional information c to guide the learning of velocity field v_θ . Furthermore, a shortcut constraint is introduced, enabling the model to predict the average velocity over a time interval Δt .

a conditional input to the velocity field to stabilize direction prediction during large-step updates.

Even with tighter coupling, residual trajectory curvature, induced by the ill-posed nature of face restoration under complex degradations and semantic ambiguity, limits the robustness of one-step inference [11, 12]. To address this, we integrate a shortcut constraint [13] into our coupling FM framework, shifting the learning objective from instantaneous to average velocity prediction over arbitrary time intervals. This is enforced through self-consistency: a single long step must match the composition of multiple shorter steps. As a result, the model implicitly learns to anticipate and compensate for residual curvature, enabling stable and accurate one-step updates even when transport paths are not perfectly linear (Fig.1(d)).

Our contributions can be summarized as follows:

- 1) We propose a novel FM framework for face restoration that establishes a *data-dependent coupling*, explicitly modeling the LQ–HQ dependency to minimize path crossovers and promote near-linear transport.
- 2) We employ *conditional mean estimation* to derive a coarse reconstruction that serves dual roles: refining the source anchor to tighten coupling and conditioning the velocity field to stabilize large-step updates.
- 3) We introduce a *shortcut constraint* that supervises average velocities over arbitrary time intervals, enabling stable and accurate one-step inference.
- 4) Extensive experiments demonstrate that our method achieves SOTA one-step face restoration quality with efficiency comparable to non-iterative baselines.

2. METHODOLOGY

This section details SCFlowFR framework for efficient one-step face restoration, as illustrated in Fig. 2.

2.1. Background on FM

FM [8, 7] learns a parameterized velocity field $v_\theta(x, t)$ that defines a probability flow ordinary differential equation (ODE):

$$\frac{d\mathbf{x}_t}{dt} = \mathbf{v}_\theta(\mathbf{x}_t, t), \quad t \in [0, 1], \quad (1)$$

transforming samples from a source distribution ρ_0 (e.g., isotropic Gaussian) to a target data distribution ρ_1 . In standard unconditional FM, source and target samples are assumed independent, i.e., the coupling is factorized as $\rho(\mathbf{x}_0, \mathbf{x}_1) = \rho_0(\mathbf{x}_0)\rho_1(\mathbf{x}_1)$. Under this assumption, training typically uses straight-line interpolants $(1-t)\mathbf{x}_0 + t\mathbf{x}_1$ to define target velocities. However, because \mathbf{x}_0 and \mathbf{x}_1 are arbitrarily paired, their interpolated paths frequently cross at intermediate times, as illustrated in Fig. 1(a). Since ODE flows are deterministic and non-intersecting, the model must warp these paths into complex, winding trajectories—forcing v_θ to be highly nonlinear, as illustrated in Fig. 1(b), which harms both learning accuracy and integration stability.

2.2. Coupling FM for Face Restoration

A core contribution of SCFlowFR is to establish a data-dependent coupling between the source and target distributions, tailored for the inherent pairing in face restoration. LQ and HQ images share substantial semantic and structural content despite degradations, enabling a coupled transport where the source distribution is conditioned on the target.

Following recent practices in generative models [9, 3], we model this coupling in a compact latent space. Let $\mathcal{E}(\cdot)$ denote a pretrained encoder that maps images to latent representations, and $\mathcal{D}_{\text{deg}}(\cdot)$ represent the degradation process such that $\text{LQ} = \mathcal{D}_{\text{deg}}(\text{HQ})$. We define the HQ latent as $\mathbf{z}_1 = \mathcal{E}(\text{HQ})$, drawn from the target distribution $\rho_1(\mathbf{z}_1)$. For each \mathbf{z}_1 , we construct a conditional source latent \mathbf{z}_0 by encoding the corresponding LQ input, and define the joint coupling as

$$\rho(\mathbf{z}_0, \mathbf{z}_1) = \rho(\mathbf{z}_1) \rho(\mathbf{z}_0 | \mathbf{z}_1), \quad (2)$$

where $\rho(z_0 | z_1)$ is a narrow distribution (e.g., isotropic Gaussian) centered at the encoded degraded image. Specifically,

$$z_0 = \mathcal{E}(\mathcal{D}_{\text{deg}}(\text{HQ})) + \varepsilon, \quad \varepsilon \sim \mathcal{N}(0, \sigma^2 \mathbf{I}), \quad (3)$$

with small variance $\sigma \in [0.03, 0.08]$ ensuring smooth density while preserving tight coupling. This coupling yields two key advantages: 1) straighter trajectories with reduced velocity nonlinearity; and 2) tighter control over the transport cost.

Advantage 1: Straighter trajectories. Given the coupled pair (z_0, z_1) , we define the time-dependent interpolation as

$$z_t = (1-t)z_0 + tz_1, \quad t \in [0, 1], \quad (4)$$

which defines a straight-line path in latent space. The resulting marginal density $\rho_t(z)$ at time t smoothly bridges ρ_0 and ρ_1 , and satisfies the continuity equation [14]

$$\partial_t \rho_t(z) + \nabla \cdot (v_t(z) \rho_t(z)) = 0, \quad (5)$$

where the target velocity field is given by

$$v_t(z) = \mathbb{E}[\dot{z}_t | z_t = z] = \mathbb{E}[z_1 - z_0 | z_t = z]. \quad (6)$$

Due to the narrow conditional source distribution, this conditional expectation is nearly constant along each path, yielding a significantly less nonlinear velocity field compared to unconditional matching.

Advantage 2: Tighter transport cost control. Let Z_t denote the solution to the probability flow ODE $\dot{Z}_t = v_t(Z_t)$ with initial condition $Z_0 = z_0 \sim \rho(z_0)$. The expected squared displacement between the generated sample Z_1 and its starting point z_0 is upper-bounded by the kinetic energy of the transport:

$$\mathbb{E}_{z_0} \|Z_1 - z_0\|^2 \leq \int_0^1 \mathbb{E}[\|\dot{z}_t\|^2] dt = \mathbb{E}[\|z_1 - z_0\|^2], \quad (7)$$

where the inequality follows from the Cauchy-Schwarz inequality applied to the time-integrated velocity over the unit interval [8]. By centering the conditional source on a semantically aligned degraded latent with small added noise, our tight coupling minimizes this bound, yielding more efficient and stable transport.

2.3. Conditional Mean Estimation for Tight Coupling

While the data-dependent coupling described above significantly reduces the transport cost compared to random pairing, the tightness of the bound in Eq. (7) still depends critically on how well the source latent z_0 aligns with the target z_1 . Under complex real-world degradations—such as heavy blur, noise, or compression—the raw LQ observation often lacks reliable structural cues, causing its encoded latent $\mathcal{E}(\text{LQ})$ to deviate significantly from z_1 , which inflates the transport cost bound.

To mitigate this, we observe that $\mathbb{E}[\|z_1 - z_0\|^2]$ is minimized when z_0 is centered at the conditional mean

$\mathbb{E}[z_1 | \text{LQ}]$. Although this mean is intractable, a regression-based restorer τ_ϕ , trained with ℓ_2 loss on synthetic data, provides a practical approximation:

$$c = \mathcal{E}(\tau_\phi(\text{LQ})) \approx \mathbb{E}[\mathcal{E}(\text{HQ}) | \text{LQ}], \quad (8)$$

which serves as a more accurate center for the source distribution. We therefore redefine the conditional source distribution as

$$\rho(z_0 | z_1) = \mathcal{N}(c, \sigma^2 \mathbf{I}), \quad (9)$$

further tightening the upper bound in Eq. (7), yielding straighter trajectories and a smoother velocity field.

In addition to centering the source distribution for tighter transport, c is further leveraged as a conditioning signal for the velocity network $v_\theta(z_t, t, c)$, providing crucial guidance for accurate velocity estimation. Consequently, we train v_θ to approximate the target velocity field in Eq. (6) by regressing the ground-truth displacement $z_1 - z_0$:

$$\mathcal{L}_{\text{FM}}(\theta) = \mathbb{E}_{z_0, z_1, t} \|\mathbf{v}_\theta(z_t, t, c) - (z_1 - z_0)\|^2. \quad (10)$$

2.4. Shortcut Constraints for One-Step Inference

Although our tight coupling (Sec.2.3) yields nearly straight trajectories, a direct one-step integration still suffers from endpoint error due to imperfect velocity estimation and the inherent truncation of coarse discretization. To address this, we introduce a shortcut constraint [13] that explicitly corrects this bias, enabling high-fidelity one-step inference.

To enable accurate large-step integration, we equip the velocity network with step-size awareness: instead of predicting only the instantaneous velocity, v_θ learns to output the *average velocity* over an arbitrary step size Δt , i.e.,

$$z'_{t+\Delta t} = z_t + \mathbf{v}_\theta(z_t, t, c, \Delta t) \cdot \Delta t. \quad (11)$$

As $\Delta t \rightarrow 0$ the shortcut direction reduces to the instantaneous velocity field in FM; for $\Delta t > 0$, the model predicts motion over larger increments.

We achieve this by leveraging the self-consistency of shortcut constraints, ensuring that one shortcut step of size $2\Delta t$ from state z_t equals two consecutive steps of size Δt , i.e., $\mathbf{v}_\theta(z_t, t, c, 2\Delta t)$ should match $\mathbf{v}_\theta^{\text{target}}$,

$$\mathbf{v}_\theta^{\text{target}} = [\mathbf{v}_\theta(z_t, t, c, \Delta t) + \mathbf{v}_\theta(z'_{t+\Delta t}, t + \Delta t, c, \Delta t)]/2. \quad (12)$$

The corresponding training objective \mathcal{L}_{SC} is given by:

$$\mathcal{L}_{\text{SC}}(\theta) = \mathbb{E}_{z_0, z_1, t, \Delta t} \|\mathbf{v}_\theta(z_t, t, c, 2\Delta t) - \mathbf{v}_\theta^{\text{target}}\|^2. \quad (13)$$

During training, each batch is divided into two subsets: one optimizes the FM loss (Eq. 10) with $\Delta t = 0$, and the other enforces the shortcut constraint (Eq. 13) with randomly sampled $\Delta t > 0$, jointly learning an LQ-to-HQ mapping with consistent dynamics across step sizes.

Table 1. Quantitative results on the CelebA-Test dataset. Among all one-step methods, best in red, second-best in blue.

Type	Method	Steps	Efficiency		Quality Metrics				
			Params(M) ↓	FPS ↑	FID ↓	PSNR(dB) ↑	LPIPS ↓	MUSIQ ↑	BRISQUE ↓
Multi-step	DiffBIR [3]	50	1667	0.11	16.91	24.15	0.30	76.05	-1.09
	StableSR [4]	30	1410	5.80	16.96	24.33	0.27	71.56	20.64
	PMRF [15]	25	183	2.85	21.70	23.59	0.31	61.79	24.49
	FlowIE [9]	5	1717	1.17	17.10	23.45	0.27	73.38	2.28
One-step	DMDNet [16]	1	40	8.40	29.85	24.09	0.30	69.76	19.26
	RestoreFormer [17]	1	17	22.96	21.22	23.27	0.30	72.55	-4.69
	OSEDiff [18]	1	1775	3.91	24.27	23.12	0.27	70.23	18.95
	SCFlowFR-Tiny (Ours)	1	96	34.32	16.36	24.25	0.31	69.71	0.90
	SCFlowFR (Ours)	1	405	8.62	15.62	24.26	0.29	72.66	-1.54

During inference, given an LQ image, we compute $\mathbf{c} = \mathcal{E}(\tau_\phi(\text{LQ}))$, sample $\mathbf{z}_0 \sim \mathcal{N}(\mathbf{c}, \sigma^2 \mathbf{I})$, and take a single step:

$$\hat{\mathbf{z}}_1 = \mathbf{z}_0 + \mathbf{v}_\theta(\mathbf{z}_0, 0, \mathbf{c}, \Delta t = 1), \quad (14)$$

which is passed through a pretrained decoder \mathcal{D} to produce the restored HQ image.

3. EXPERIMENTS

3.1. Experiment Setups

Datasets. We train SCFlowFR on the Flickr-Faces-HQ (FFHQ) dataset [19], which contains 70,000 HR images. All images are resized to 512×512 resolution before training. During evaluation, we first assess SCFlowFR performance on the synthetic dataset CelebA-Test [20], which contains 3,000 paired HQ and LQ images. To further validate the generalization capability of SCFlowFR in real-world scenarios, we conduct additional experiments on three wild datasets: LFW-Test [21], CelebChild-Test [21], and WebPhoto-Test [21], all of which comprise facial images affected by varying degrees of degradation.

Training Details. For both training and evaluation, we used the synthetic degradation pipeline of Codeformer [21]. A pre-trained SwinIR [22] served as the conditional mean estimator τ_ϕ , while \mathbf{v}_θ was implemented as a U-Net [23]. The parameters of SwinIR and the VAE were frozen. Training was performed with a batch size of 16 for 200k iterations using the Adam optimizer and a learning rate 1×10^{-4} . Exponential moving average (EMA) parameters were used to generate self-consistency targets $\mathbf{v}_\theta^{\text{target}}$ for stable training. Moreover, we trained a lightweight variant, SCFlowFR-Tiny, by replacing the VAE and U-Net with compact architectures¹, training it for 150k iterations under the same settings.

Metrics. On synthetic datasets, we employed full-reference image assessment metrics including FID, PSNR, and LPIPS and no-reference metrics, MUSIQ [24] and BRISQUE [25]. For wild datasets, evaluation was conducted exclusively using the no-reference metrics NIQE and

BRISQUE. Efficiency was assessed via comparisons of parameter counts and inference throughput (FPS).

3.2. Comparisons with State-of-the-Art Methods

We compare our method with the following baselines: DMDNet [16], RestoreFormer [17], StableSR [4], DiffBIR [3], OSEDiff [18], PMRF [15], and FlowIE [9]. For comparison, we categorize them by inference steps: DMDNet, RestoreFormer, and OSEDiff are one-step methods, while StableSR, DiffBIR, PMRF, and FlowIE are multi-step methods.

CelebA-Test. As shown in Table 1, among one-step methods, our SCFlowFR achieves the best scores on key metrics including FID, PSNR, and MUSIQ, while securing second-best results on the remaining ones, demonstrating its comprehensive restoration quality. The lightweight variant, SCFlowFR-Tiny, also ranks highly within this category, confirming that a compact architecture retains strong perceptual performance. More importantly, compared to computationally expensive multi-step approaches, our method establishes a superior efficiency-quality trade-off: it accomplishes top-tier restoration in just a single step, with a parameter count comparable to GAN-based models and a runtime that is orders of magnitude faster than iterative diffusion or FM counterparts. This enables high-quality face restoration in real-time or resource-constrained scenarios. We further present qualitative results in Fig. 3. SCFlowFR effectively preserves crucial image information, avoiding the over-generation or distortion caused by noise interference, while successfully restoring fine-grained details. Notably, it achieves a level of visual fidelity comparable to that of multi-step inference models, resulting in realistic and highly faithful restoration.

Wild Datasets. We conducted comparative experiments using the four-step inference results from both SCFlowFR and its lightweight variant, benchmarking against relevant SOTA methods. As shown in Table 2, SCFlowFR-Tiny achieves superior NIQE and BRISQUE scores across nearly all three wild datasets. Notably, its advantage over the larger variant can be attributed to the compact architecture being better matched to the mild, less structured degradations typi-

¹<https://github.com/madebyollin/taesd>



Fig. 3. Qualitative comparisons on the CelebA-Test dataset.

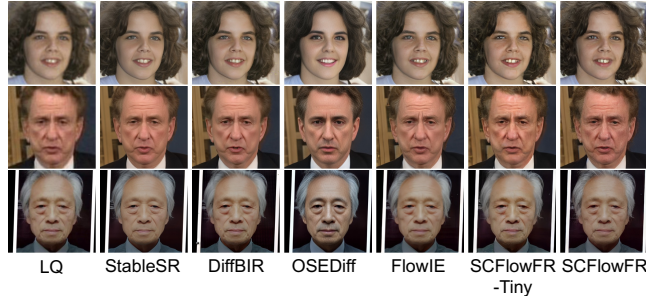


Fig. 4. Qualitative comparisons on three wild datasets. From top to bottom: samples from the CelebChild, LFW, and WebPhoto datasets, respectively.

cal of real-world images, thus avoiding over-parameterization and yielding more natural restoration. As illustrated in Fig. 4, our approach excels in restoring fine facial details, generating more realistic hair strands with clearer textures and preserving authentic skin texture with wrinkles. These visual improvements align with the quantitative gains, demonstrating the model’s ability to produce perceptually convincing reconstructions in unconstrained wild scenarios.

Table 2. No-reference metrics on three wild datasets. Best in red, second-best in blue. “BR.” denotes BRISQUE.

Method	LFW		CelebChild		WebPhoto	
	NIQE↓	BR.↓	NIQE↓	BR.↓	NIQE↓	BR.↓
StableSR [4]	5.24	-0.22	4.91	3.23	5.78	2.02
DiffBIR [3]	5.68	-3.09	5.48	1.40	6.01	4.58
OSEDiff [18]	4.72	2.78	5.07	9.82	5.26	5.89
FlowIE [9]	4.27	1.16	4.44	7.39	4.80	6.83
SCFlowFR	4.11	-1.01	4.25	3.23	4.38	2.89
SCFlowFR-Tiny	3.96	1.65	4.04	0.82	4.23	1.97

3.3. Ablation Studies

Discussion on Training Strategies. To validate the necessity of the shortcut training strategy and investigate the impact of different training strategies on performance, we designed corresponding ablation studies. First, we compared a

Table 3. Ablation studies on the CelebA-Test dataset. Best performance is highlighted in red.

Method	Steps	FID↓	PSNR(dB)↑	BRISQUE↓
Model-w/o- \mathcal{L}_{SC}	1	287.23	20.85	51.22
Model-w/- \mathcal{L}_{consis}	5	18.54	24.04	3.17
Model-w/o-cond	1	19.01	23.08	1.55
Ours	1	16.36	24.25	0.90

model trained solely with the \mathcal{L}_{FM} loss, denoted as Model-w/o- \mathcal{L}_{SC} . As shown in Table 3, the results demonstrate significantly degraded performance. Second, we evaluated the training strategy proposed by Consistency-FM [26], denoted as Model-w/- \mathcal{L}_{consis} . Since the model failed to achieve satisfactory performance under one-step inference, we report its five-step results, which still indicate inadequate performance.

Discussion on Conditional Guidance. Our conditional guidance strategy leverages a pre-restored image as the contextual input to the velocity network, providing a semantically aligned prior for the HQ target. To verify its contribution, we train an ablated model that removes this conditional branch, denoted Model-w/o-cond. As shown in Table 3, the absence of conditional guidance leads to consistent degradation in FID, PSNR, and BRISQUE, confirming that the pre-restored image as a conditional signal is essential for achieving accurate and robust one-step restoration.

4. CONCLUSION

We propose SCFlowFR, a face restoration method based on shortcut-enhanced coupling FM. Unlike conventional approaches starting from Gaussian noise, SCFlowFR establishes data-dependent coupling by centering the source on a coarse reconstruction from the LQ input and uses it for conditional guidance—reducing path crossovers and promoting near-linear transport. A shortcut constraint enforces self-consistency via average velocity supervision, enabling accurate one-step inference. Experiments show SCFlowFR achieves SOTA one-step quality with efficiency comparable to non-iterative baselines. Future work will extend this framework to general image restoration and inpainting to enhance robustness and versatility.

5. REFERENCES

- [1] Zongsheng Yue, Jianyi Wang, and Chen Change Loy, “Resshift: Efficient diffusion model for image super-resolution by residual shifting,” *Advances in Neural Information Processing Systems*, vol. 36, pp. 13294–13307, 2023.
- [2] Rongyuan Wu, Tao Yang, Lingchen Sun, Zhengqiang Zhang, Shuai Li, and Lei Zhang, “Seesr: Towards semantics-aware real-world image super-resolution,” in *Proceedings of the IEEE/CVF conference on computer vision and pattern recognition*, 2024, pp. 25456–25467.
- [3] Xinqi Lin, Jingwen He, Ziyang Chen, Zhaoyang Lyu, Bo Dai, Fanghua Yu, Yu Qiao, Wanli Ouyang, and Chao Dong, “Diffbir: Toward blind image restoration with generative diffusion prior,” in *European conference on computer vision*. Springer, 2024, pp. 430–448.
- [4] Jianyi Wang, Zongsheng Yue, Shangchen Zhou, Kelvin CK Chan, and Chen Change Loy, “Exploiting diffusion prior for real-world image super-resolution,” *International Journal of Computer Vision*, vol. 132, no. 12, pp. 5929–5949, 2024.
- [5] Simian Luo, Yiqin Tan, Longbo Huang, Jian Li, and Hang Zhao, “Latent consistency models: Synthesizing high-resolution images with few-step inference,” *arXiv preprint arXiv:2310.04378*, 2023.
- [6] Tianwei Yin, Michaël Gharbi, Richard Zhang, Eli Shechtman, Fredo Durand, William T Freeman, and Taesung Park, “One-step diffusion with distribution matching distillation,” in *Proceedings of the IEEE/CVF conference on computer vision and pattern recognition*, 2024, pp. 6613–6623.
- [7] Yaron Lipman, Ricky TQ Chen, Heli Ben-Hamu, Maximilian Nickel, and Matt Le, “Flow matching for generative modeling,” in *11th International Conference on Learning Representations, ICLR*, 2023.
- [8] Xingchao Liu, Chengyue Gong, and Qiang Liu, “Flow straight and fast: Learning to generate and transfer data with rectified flow,” in *International Conference on Learning Representations*, 2023.
- [9] Yixuan Zhu, Wenliang Zhao, Ao Li, Yansong Tang, Jie Zhou, and Jiwen Lu, “Flowie: Efficient image enhancement via rectified flow,” in *Proceedings of the IEEE/CVF Conference on Computer Vision and Pattern Recognition*, 2024, pp. 13–22.
- [10] Ségolène Martin, Anne Gagneux, Paul Hagemann, and Gabriele Steidl, “Pnp-flow: Plug-and-play image restoration with flow matching,” *arXiv preprint arXiv:2410.02423*, 2024.
- [11] Johannes Schusterbauer, Ming Gui, Pingchuan Ma, Nick Stracke, Stefan Andreas Baumann, Vincent Tao Hu, and Björn Ommer, “Fmboost: Boosting latent diffusion with flow matching,” in *European Conference on Computer Vision*. Springer, 2024, pp. 338–355.
- [12] Elad Cohen, Idan Achituve, Idit Diamant, Arnon Netzer, and Hai Victor Habi, “Efficient image restoration via latent consistency flow matching,” *arXiv preprint arXiv:2502.03500*, 2025.
- [13] Kevin Frans, Danijar Hafner, Sergey Levine, and Pieter Abbeel, “One step diffusion via shortcut models,” in *The Thirteenth International Conference on Learning Representations*, 2025.
- [14] Michael Samuel Albergo, Mark Goldstein, Nicholas Matthew Boffi, Rajesh Ranganath, and Eric Vanden-Eijnden, “Stochastic interpolants with data-dependent couplings,” in *International Conference on Machine Learning*. PMLR, 2024, pp. 921–937.
- [15] Guy Ohayon, Tomer Michaeli, and Michael Elad, “Posterior-mean rectified flow: Towards minimum mse photo-realistic image restoration,” in *International Conference on Learning Representations*, 2025.
- [16] Xiaoming Li, Shiguang Zhang, Shangchen Zhou, Lei Zhang, and Wangmeng Zuo, “Learning dual memory dictionaries for blind face restoration,” *IEEE Transactions on Pattern Analysis and Machine Intelligence*, vol. 45, no. 5, pp. 5904–5917, 2022.
- [17] Zhouxia Wang, Jiawei Zhang, Runjian Chen, Wenping Wang, and Ping Luo, “Restoreformer: High-quality blind face restoration from undegraded key-value pairs,” in *Proceedings of the IEEE/CVF conference on computer vision and pattern recognition*, 2022, pp. 17512–17521.
- [18] Rongyuan Wu, Lingchen Sun, Zhiyuan Ma, and Lei Zhang, “One-step effective diffusion network for real-world image super-resolution,” *Advances in Neural Information Processing Systems*, vol. 37, pp. 92529–92553, 2024.
- [19] Tero Karras, Samuli Laine, and Timo Aila, “A style-based generator architecture for generative adversarial networks,” in *Proceedings of the IEEE/CVF conference on computer vision and pattern recognition*, 2019, pp. 4401–4410.
- [20] Ziwei Liu, Ping Luo, Xiaogang Wang, and Xiaoou Tang, “Deep learning face attributes in the wild,” in *Proceedings of the IEEE international conference on computer vision*, 2015, pp. 3730–3738.
- [21] Xintao Wang, Yu Li, Honglun Zhang, and Ying Shan, “Towards real-world blind face restoration with generative facial prior,” in *Proceedings of the IEEE/CVF conference on computer vision and pattern recognition*, 2021, pp. 9168–9178.
- [22] Jingyun Liang, Jie Zhang Cao, Guolei Sun, Kai Zhang, Luc Van Gool, and Radu Timofte, “Swinir: Image restoration using swin transformer,” in *Proceedings of the IEEE/CVF international conference on computer vision*, 2021, pp. 1833–1844.
- [23] Olaf Ronneberger, Philipp Fischer, and Thomas Brox, “U-net: Convolutional networks for biomedical image segmentation,” in *International Conference on Medical image computing and computer-assisted intervention*. Springer, 2015, pp. 234–241.
- [24] Junjie Ke, Qifei Wang, Yilin Wang, Peyman Milanfar, and Feng Yang, “Musiq: Multi-scale image quality transformer,” in *Proceedings of the IEEE/CVF international conference on computer vision*, 2021, pp. 5148–5157.
- [25] Anish Mittal, Anush Krishna Moorthy, and Alan Conrad Bovik, “No-reference image quality assessment in the spatial domain,” *IEEE Transactions on image processing*, vol. 21, no. 12, pp. 4695–4708, 2012.
- [26] Ling Yang, Zixiang Zhang, Zhilong Zhang, Xingchao Liu, Minkai Xu, Wentao Zhang, Chenlin Meng, Stefano Ermon, and Bin Cui, “Consistency flow matching: Defining straight flows with velocity consistency,” *arXiv preprint arXiv:2407.02398*, 2024.